ENHANCED ZONE-MELTING RECRYSTALLIZATION FOR CRYSTALLINE SILICON THIN-FILM SOLAR CELLS

T. Kieliba, S. Reber
Fraunhofer-Institute for Solar Energy Systems (ISE), Oltmannsstrasse 5, D-79100 Freiburg
Tel. +49-761-4588-247, Fax +49-761-4588-250, E-mail: kieliba@ise.fhg.de

ABSTRACT: For zone-melting recrystallization of thin Si films the effects of preheating temperature and focussed lamp intensity on solidification front morphology and defect structure are studied. Subgrain boundaries are the dominating defect type and limit the base diffusion length. *In-situ* observation of the melt zone shows that cellular growth leads to films with regular spaced subgrain boundaries and low defect density. These films are preferentially (100)-orientated. Crystalline Si thin film solar cells with a random pyramid front side texture were processed from this material resulting in efficiencies up to 12.8 %.
Keywords: Recrystallization - 1: Thin Film - 2: Silicon - 3

1. INTRODUCTION

The idea to recrystallize thin layers by moving a small molten zone was patented in 1950 [1] and first used to crystallize materials with a low melting point like germanium or indium-antimonide [2]. In the 1980s the zone-melting recrystallization (ZMR) technique was applied to thin silicon layers in connection with the preparation of silicon films on insulators (SOI). ZMR is also used to recrystallize Si films for crystalline silicon thin-film (CSiTF) solar cells. Efficiencies up to 16.4 % achieved by Mitsubishi Corporation show the potential of this technique [3,4]. While this group uses polished and thermally oxidized Czochralski wafers as substrate (intended to be reused), our concept focuses on ceramics or silicon ribbons as substrate material.

To improve Si layer quality on these materials the influence of preheating temperature and focussed lamp intensity on layer quality was studied using standard multicrystalline Si wafers and Silicon Sheets from Powder as test substrate.

2. EXPERIMENTAL

2.1 Zone-Melting Recrystallization System

The experimental set-up used for ZMR was modified recently and is described in [5]. The main features of our system are a large area lower heater, an integrated CCD camera and computer controlled processing. The lower heater allows homogeneous preheating of the sample up to temperatures between 700°C and 1400°C. The integrated CCD camera enables *in-situ* observation of melt zone and solidification front with a resolution up to 15 µm, depending on the lenses used.

2.2 Sample Preparation

Experiments were carried out using two different kinds of Si substrates: standard multicrystalline Si wafers (Bayer SILSO™) and Silicon Sheets from Powder (SSP) produced at Fraunhofer ISE. After cleaning the wafers with a CP-133 etch they were coated with 2 µm of SiO_2 deposited by plasma-enhanced chemical vapor deposition (PECVD). A 5 to 15 µm thick highly doped (5×10^{18} cm^{-3}) Si layer was then deposited in an optically heated CVD reactor. To prevent agglomeration of Si during recrystallization ("balling up") the film was capped with an additional PECVD-SiO_2 layer of 2 µm thickness.

After recrystallization the SiO_2 capping was removed with HF followed by an additional CP-133 etch. The recrystallized layer was then thickened epitaxially in the same system used for the first Si deposition. Doping concentration for this layer was 3×10^{16} cm^{-3} and film thickness varied between 10 and 25 µm.

The recrystallized and epitaxially thickened samples were analyzed by preparing polished surfaces and cross sections and by processing test solar cells.

The samples utilized for fabrication of solar cells were processed according to the scheme shown in Figure 1. Light trapping was realized by alkaline etching of the preferentially (100)-oriented layer (see section 3.2). After emitter diffusion from $POCl_3$ a remote plasma hydrogen passivation (RPHP) was applied. Since the SiO_2 intermediate layer is non-conducting, both emitter and base contact metallization had to be formed on the front side. Thus after evaporating and electroplating the emitter grid, a trench separating emitter and base was formed around the active cell area using reactive ion etching (RIE). The aluminum metallization was then evaporated into this trench. Sufficient lateral conduction in the base is enabled by the highly doped recrystallized layer which also functions as back surface field (BSF). In previous experiments it turned out that a second hydrogen passivation can be beneficial to the cell performance [5]. Therefore sintering of the contacts

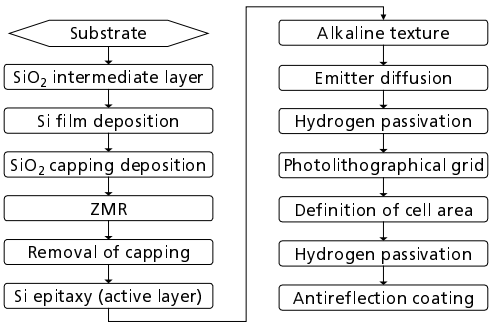

Figure 1: Process used to fabricate test solar cells.

was replaced by a further RPHP step. Finally a MgF/TiO_2 double layer antireflection coating was deposited.

3. RESULTS AND DISCUSSION

Both theoretical models and experiments show, that the temperature gradient at the solidification front is of major importance for the crystallographic quality of thin zone-melting recrystallized silicon layers [2]. The influence of three factors on this gradient, preheating temperature, substrate thickness and focussed lamp intensity, will be discussed.

3.1 Effects of Preheating Temperature

In order to get a qualitative idea on how the preheating temperature effects the lateral temperature distribution, thermocouples (TCs) were glued into small dips on the surface of samples prepared with SiO_2 intermediate layer, Si film and SiO_2 capping. Temperature data was recorded while scanning the zone melting heater across these samples. An interpretation of these data has to be aware of the limitations of this set-up: first the measurement is restrained to temperatures below the melting point of Si, thus the change of thermal properties with transition from solid to liquid state is not considered. Second the dimension of the TCs weld (0.3 mm approx.) is larger than the Si film thickness and therefore the TC is in contact with both, Si film and substrate. The actual thermal gradients are expected to be higher in the Si film than in the substrate because of the insolating properties of the SiO_2 intermediate layer. Further, the curves taken are the convolution of the actual temperature distribution and a boxcar function with width equal to the TC's diameter.

In Figure 2 the temperature distribution for different ratios of lower heater power and focussed lamp power is shown for a SILSO™ substrate. The values were chosen in such way that a maximum temperature of approximately 1300°C was reached. Increasing the preheating power from 30 % to 50 % the maximum gradient decreased from 30 K/mm to 14 K/mm. Lower heater power of 30 %, 40 % and 50 % correspond to preheating temperatures of 910°C, 1060°C and 1200°C respectively.

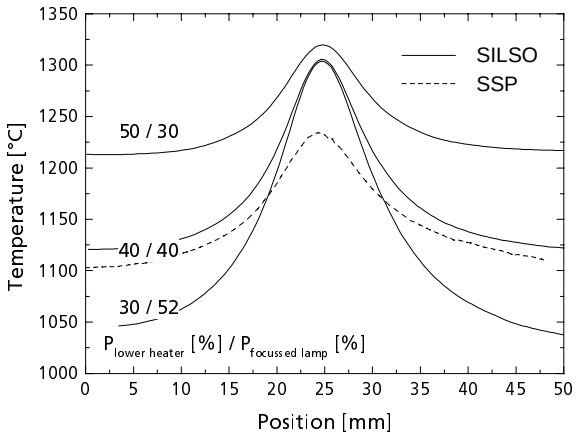

Figure 2: Lateral temperature distribution in the substrate for different ratios of lower heater power and focussed lamp power. Solid lines are for SILSO™ substrates, the dashed one is for a SSP substrate and the ratio 40/40.

For the 40/40 ratio in addition the distributions in the SILSO™ (thickness ~ 300 µm) and a SSP substrate (thickness ~ 800 µm) are compared. While the preheating temperature of Si substrates does not depend on wafer thickness (the material is opaque for temperatures higher than 800°C [6]) the increasing lateral heat conduction with increasing substrate thickness smoothens the gradient.

Although low temperature gradient are desired, control of the melt zone becomes more difficult at high preheating temperatures (Figure 3). With increasing preheating temperature the system becomes more sensitive to changes in focussed lamp power. For a lower heater power of 40 % a 1 % change (absolute) in focussed lamp power results in a change of melt zone width of 0.2 mm. For a lower heater power of 60 % the change in melt zone width for the same shift in focused lamp power is five times as high (1.1 mm). Further a linear relationship between focussed lamp power and melt width was found, as long as the substrate did not melt down to the bottom. This result is in accordance with theoretical calculations carried out by Robinson *et. al.* [7].

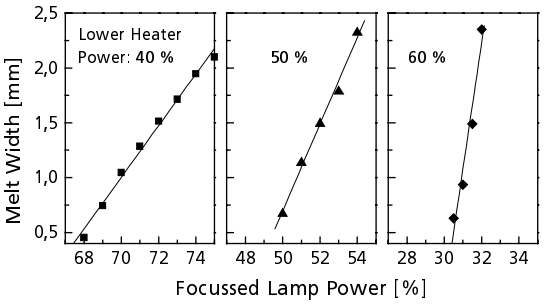

Figure 3: Dependence of melt zone width from melt lamp power for three different preheating temperatures.

For an optimization of preheating temperature a compromise between the two competitive effects described above has to be found. Solar cells were produced from material recrystallized with preheating temperatures of 910°C, 1060°C and 1200°C. While no significant difference in crystallographic and electric properties was found for the two later values samples recrystallized at 910°C were of minor quality.

In Figure 4 the surface sections of a typical sample preheated to 910°C is compared with one preheated to 1060°C. The dominating defects are lines with high dislocation density in the epitaxial layer induced by subboundaries in the recrystallized layer. For Sample A the average spacing between two subboundary lines is smaller than for Sample B. In addition epitaxial stacking faults and twin grain boundaries can be found on the surface of Sample A. Although the difference in defect density must not solely be caused by the preheating temperature the tendency shown was observed generally. Therefore preheating temperatures around 1100°C were used for following experiments.

The surface sections in Figure 4 are compared with diffusion length topographies measured with the spectrally resolved light beam induced current (SR-LBIC) method. These maps reproduce the defect structure found on the surface sections. In the map of Sample B areas with rela-

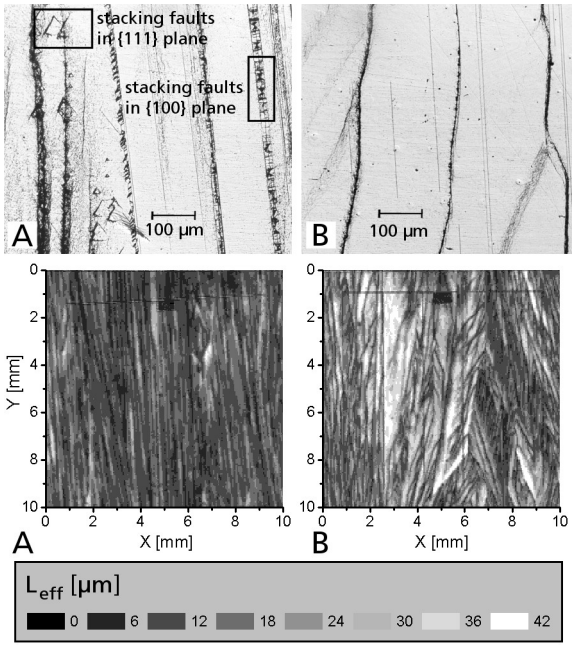

Figure 4: Top: Secco etched surface sections of samples recrystallized with a preheating temperatures of 910°C (A) and 1060°C (B). Bottom: SR-LBIC diffusion length maps of solar cells fabricated from these materials.

tively low defect density can be localized. Therefore the mean effective diffusion length of this sample is higher than the one of Sample B.

3.2 Effects of Focussed Lamp Power

Not only does the preheating temperature determine the temperature gradient at the solidification front. A most important role plays the peak intensity and power distribution of the focussed lamp. In Figure 5 a melt zone with varying width is shown. This zone was created by tilting the focal line by a small angle relative to the sample's plane. With this set-up the temperature gradient at the solidification front is expected to decrease with decreasing melt width. Two explanations shall be given: First, if the focus does not coincide with the Si film the intensity profile is smoothed. Second, numerical simulations carried out by Robinson and Miaoulis show that not only the melt width but also the temperature gradient increases with increasing peak intensity [7]. The melt zone in Figure 5 can be roughly divided into three regions characterized by different solidification front morphologies. In Region II a cellular morphology is observed. The triangular form indicates that the facets of the cells are build up of {111} planes resulting in a (100)-orientation perpendicular to the surface (see insert). Preferential growth with this orientation is attributed to the anisotropy in surface free energy [8]. In this region the solidification front was stable with time and resulted in crystallites with parallel subgrain boundaries (marked A and B in the photograph of the epitaxial layer). The spacing between two subboundaries is equal to the distance between two edges of the cellular front. In contrast the solidification front was less stable in Region I. Subgrain boundaries did not form a regular pattern. In the third region, Region III, the Si film did not completely melt and recrystallized in a (highly reflective) microcrystalline structure.

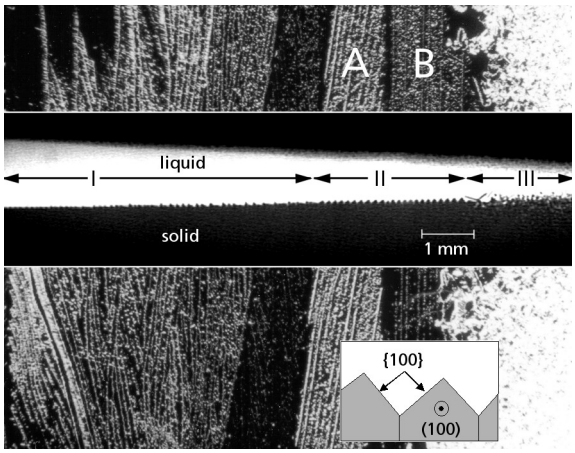

Figure 5: Correlation between morphology of the solidification front and grain structure of the epitaxial layer.

The development of a regular solidification front in Region II is consistent with the models of *constitutional supercooling* and *radiative supercooling* [2]: a small melting zone results in low temperature gradients and a wide supercooled zone. Self-organization leads to a stable cellular front. This result shows that the melt zone width is a suitable parameter to control the ZMR process.

Surface and cross sections were prepared from different areas of the sample shown in Figure 5. In the upper image of Figure 6 the positions of the sections are indicated in the photograph of the epitaxial layer. A clear correlation could be observed between solidification front morphology and defect density. In the cross section prepared from Area 1 "brushes" with high defects density can be detected. The tops of these "brushes" are visible as dark lines in the Secco etched surface sections (Area 2). For the sections of grain A and B the average spacing between two adjacent

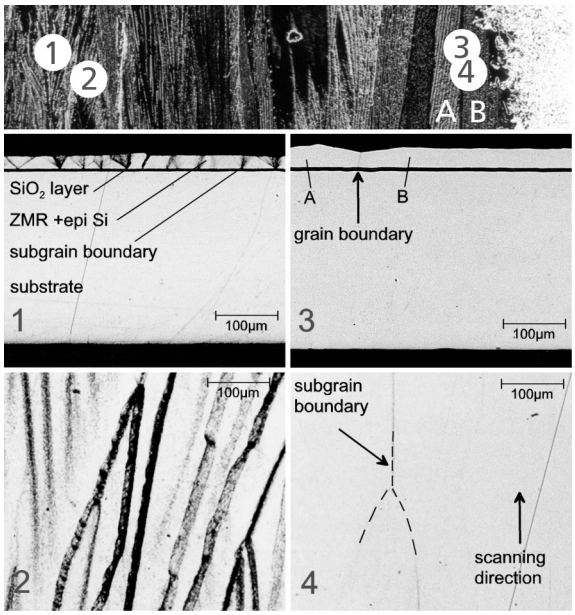

Figure 6: Surface and cross section corresponding to the areas indicated in the upper image of the epitaxial layer.

subboundaries is much wider than in Area 2. Only one subgrain boundary can be identified in Area 4. While the increase in subboundary spacing with decreasing temperature gradient follows from the theoretical considerations mentioned it is not clear yet why defect density above the subboundaries ("brushes") is much lower in the right area than in the left area.

3.3 Solar Cell Results

Thin film solar cells were fabricated from layers grown with cellular solidification front using the process described in Section 2.2. Cellular growth was mainly observed when layer thickness was less than 10 µm. SEM images of surfaces treated with an anisotropically etching KOH isopropanol solution give evidence to the fact that the orientation perpendicular to the surface is indeed an (100)-orientation. The image shown in Figure 7 is typical for the surfaces analyzed.

The best of these cells had an efficiency of 12.8 %, with V_{oc} = 589 mV, I_{sc} = 29.9 mA/cm², FF = 74.5 %, confirmed by the Fraunhofer ISE calibration laboratory. The thickness of the highly doped BSF layer and the epitaxial layer were 5 µm and 13 µm respectively. A minority carrier diffusion length of 30 µm in the base was calculated from internal quantum efficiency measurement. For cells processed without surface texture the average short circuit current was ~ 5 mA/cm² lower. This effect can be attributed to the effective light trapping by the combination of random pyramid surface and SiO_2 intermediate layer.

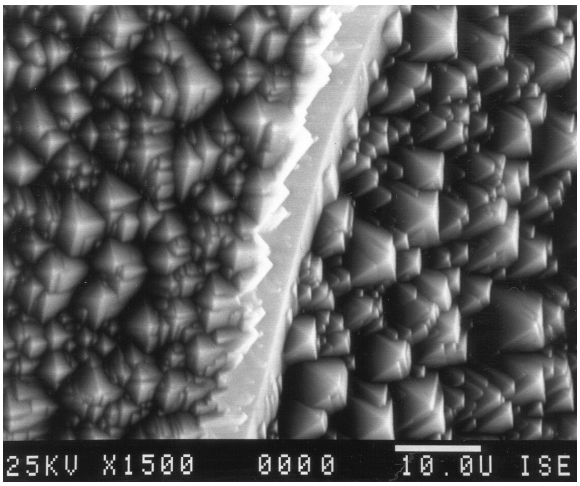

Figure 7: SEM image of a recrystallized layer after anisotropic etching. The two grains are tilted by an angle of 30° approximately.

4. SUMMARY

For ZMR of Si films the influence of preheating temperature and focussed lamp intensity was studied. Low temperature gradients, i.e. a small melting zone led to an cellular solidification front which was stable with time. "brushes" with high defect density in the epitaxial layer originating from subboundaries in the recrystallized layer were identified as dominating defect type. A clear correlation between solidification front morphology and defects structure of the crystallites grown could be made. Si film with thickness less than 10 µm resulted in preferentially (100)-oriented material. Crystalline Si thin film cells were made from these films with efficiencies up to 12.8 %.

ACKNOWLEDGEMENTS

The authors would like to thank M. Kwiatkowska, H. Lautenschlager, C. Schetter and C. Vorgrimmler for sample preparation, E. Schäffer for carrying out solar cell measurements. This work was supported by the German Federal Ministry of Economics and Technology (BMWi) in the project TEKSI and by the European Commission under contract no. JOR3-CT98-0234.

REFERENCES

[1] E. Leitz, British Patent No. 691355 (1950).
[2] E. I. Givargizov, Oriented Crystallization on Amorphous Substrates (Plenum Press, New York, 1991).
[3] A. Takami, S. Arimoto, H. Morikawa, S. Hamamoto, T. Ishihara, H. Kumabe, and T. Murotani, Proceedings of the 12th European Photovoltaic Solar Energy Conference, Amsterdam, Holland (1994) 59.
[4] H. Morikawa, Y. Nishimoto, H. Naomoto, Y. Kawama, A. Takami, S. Arimoto, T. Ishihara, and K. Namba, Sol. Ener. Mater. Sol. Cells **53** (1998) 23.
[5] S. Reber, W. Zimmermann, and T. Kieliba, Tech. Dig. 11th International Photovoltaic Science and Engineering Conference, Sapporo, Japan (1999).
[6] P. J. Timans, in *Advances in Rapid Thermal and Integrated Processing* (Kluwer Academic Publishers, Dordrecht , Boston, 1996), p. 35.
[7] R. D. Robinson and I. N. Miaoulis, J. Appl. Phys. **73** (1993) 439.
[8] D. K. Biegelsen, L. E. Fennell, and J. C. Zesch, Appl. Phys. Lett. **45** (1984) 546.